SURGE & SWAB PRESSURES ON WELLS WITH CROSS-SECTION VARIATION: A STUDY FOR NON-NEWTONIAN FLUIDS

João Victor Fedevjcyk, joaovictor88@gmail.com
Silvio Luiz de Mello Junqueira, silvio@utfpr.edu.br
Cezar Otaviano Ribeiro Negrão, negrao@utfpr.edu.br
UTFPR - Federal University of Technology - Parana – Av. Sete de Setembro, 3165, CEP 80.230-901 – Curitiba-PR - Brazil

Abstract. *Downward or upward movement of the drill pipe displaces the fluid within the well causing either under (swab) or over pressures (surge), respectively. If the pressure at the well bore overcomes the formation fracture pressure, a loss of circulation eventually occurs. On the other way, the upward movement may reduce the pressure below the pore pressure and an inflow of fluid towards the well (kick) can happen. An uncontrolled kick may cause a blowout with serious damages. The work presents a methodology for studying the behavior of the surge and swab pressures for non-Newtonian fluids (Bingham and power law) in wells with variations on its cross section. The dimensionless equations of mass conservation, momentum balance and the equation of state are discretized according to the Finite Volume Method. The flow is considered to be transient, one-dimensional, isothermal and laminar. The fluid presents constant compressibility and the bottom of the drill pipe is closed. The gain in the iterative process provided by the adimensionalisation of the equations and its consequences on the numerical results are discussed. Results showed good agreement with both literature and experimental data. It was concluded that the presence of changes in the section along the annular region results in higher pressures associated to the transient phenomena, and that is due to the reflection of the pressure wave on the well boundaries.*

Keywords*: Surge & swab pressures, drilling fluid, compressible flow, transient flow, non-Newtonian fluid.*

1. INTRODUCTION

In Figure 1, in which a schematic representation of a well bore is presented, one can see several devices attached along the drill pipe. All those devices, such as the scaled use of drill bits and other accessories connected to the drill pipe, can eventually provide variations in the annular space between the well and the drill pipe.

The drilling of an oil well requires the injection of a fluid which ensures safety to the well operation and cool down the drill bit during the perforation, to clean up the deep end of the well by removing the cuttings resulted to maintain the hydrostatic pressure over formation, avoiding the influx of fluids and to stabilizing the well bore walls (Thomas, 2001).

An important feature expected in drilling fluids is the capability of vary its viscosity under a certain shear stress. This event is very timely if the drill process is eventually halted, and the remaining cuttings, placed along the well, must not return to the bottom. Non-newtonian fluids (Bird et al.1987) present the capability of gelling, as they increase its viscosity when not submitted to stress. With this behavior, such fluids avoid the cuttings to precipitate in the bottom.

The downward movement of the drill pipe compresses the drilling fluid increasing the wellbore pressure, in a phenomenon so called surge. If this pressure rise overcomes the fracture pressure, a rupture in the well may occur, causing the drilling fluid to escape towards the formation. On the other way, if the drill pipe moves up the pressure at the wellbore reduces. Whenever such swab pressure is lower than the pore pressure, an influx of fluid may happen, in a phenomenon called kick. The loss of control of this pressure can result in a blowout event.

Several studies were conducted to predict the surge and swab pressures. These studies can be divided into steady-state and dynamic models. Steady-state models, such as Burkhardt (1961), Fontenot and Clark (1974), Bourgoyne et al. (1991), Bing et al (1995) and Sampaio Jr. (2002), considered only the viscous efffect. In the other hand the dynamic models of Lal (1983), Mitchell (1988), Bing and Kaiji (1996), Kimura (2008), Almeida (2009) and Fedevjcyk (2010) took into account both viscous and inertial effects. In a recent modeling work, Fedevjcyk (2010) showed that the variations of the well annular cross section resulted in surge and swab pressures for Newtonian fluids larger than those found in uniform cross section wells.

In this article, a mathematical model for surge and swab pressures in wells with cross section variations is developed. Differently from Fedevjcyk´s (2010), the drilling fluid is treated as either Bingham or Power law fluid. The governing equations are discretized by the Finite Volume Method (FVM) (Patankar, 1980) and they are solved iteratively. The results are compared with measured data obtained in an experimental rig. A sensitivity analysis is thus performed to show how important is the effect of the cross section variation in the surge and swab phenomena.

2. MATHEMATICAL MODEL

The geometry to be considered in the current analysis is the annular space formed by drill pipe and the borehole wall. The dimensions of the problem, such as the drill pipe, D_p, and borehole, D_h, diameters and well length, L, are indicated in Figure 2. It is worth of noting that the origin of the coordinate system is placed at the well bottom. In this simplified scheme, the drill pipe moves downwards with a constant velocity (V_p).

The transient flow is assumed to be laminar, isothermal and one-dimensional, and the compressibility is considered to be constant. The borehole is vertical and the fluid is non-Newtonian, such as Bingham and power law. The bottom of the drill pipe is closed and therefore the drilling fluid flows only through the annular space. Besides, the well bore is assumed to be impermeable and completely rigid.

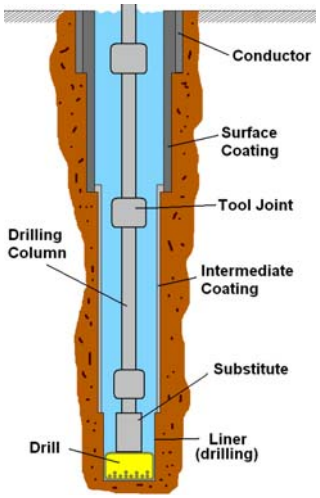

Figure 1. Schematic configuration of the oil well while drilling.

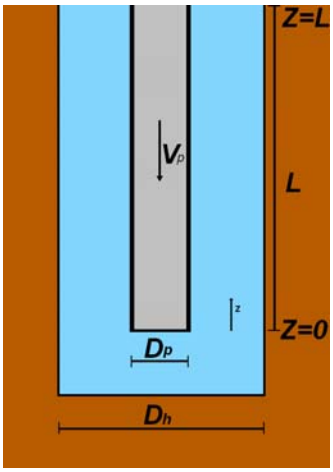

Figure 2. Annular space geometry.

2.1 Governing Equations

By applying the hypothesis above, the conservation equation of mass and momentum can be written respectively by,

$$\frac{\partial(\rho\bar{V})}{\partial z}+\frac{\partial\rho}{\partial t}=0 \tag{1}$$

$$\frac{\partial(\rho\bar{V})}{\partial t}+\frac{\partial(\rho\bar{V}\bar{V})}{\partial z}=-\frac{\partial P}{\partial z}+\frac{\pi}{A_t}(D_h\tau_h-D_p\tau_p)-\rho g \tag{2}$$

where ρ is the fluid density, $\bar{V}$ is the fluid velocity, P is the pressure, A_t is the cross-section area of the annular space, g is the gravity acceleration, and τ_h and τ_p are the shear stress at the external and internal walls, respectively. t is the time and z is the axial position. It can be noted that pressure, velocity and density are average values through the cross sectional area.

The pressure is calculated according to the definition of compressibility by the following (Anderson, 1990):

$$P=P_{atm}+\frac{1}{\alpha}\ln\left(\frac{\rho}{\rho_{atm}}\right) \tag{3}$$

where α is the fluid compressibility and the subscript atm indicates the atmospheric condition.

The shear stress term in Eq. (2) is approximated by considering a local equilibrium of pressure difference and shear stress force at walls for both Bingham and power law fluids:

2.1.1 Bingham Fluid

For the Bingham fluid, the shear stress is computed by:

$$\frac{\pi}{A_t}\left(D_h\tau_h-D_p\tau_p\right)=-\varepsilon_2\frac{\mu^2}{\rho(D_h-D_p)^3} \tag{4}$$

where μ is the fluid plastic viscosity, ε_2 is an expression that correlates the friction factor and the Reynolds number according to (Fontenot and Clark, 1974):

$$\varepsilon_2 = \frac{2He\zeta}{3} + 16\,\mathrm{Re}_{ef}\,\zeta - \frac{4}{3}\zeta\sqrt{He^2 + 16He\,\mathrm{Re}_{ef} + 64\,\mathrm{Re}_{ef}^{\,2}}\cos\left(\frac{\theta}{3} + 120^{\mathrm{o}}\right) \tag{5}$$

where θ is:

$$\theta = \arccos\left(\frac{-\zeta^3\left(24He^2\,\mathrm{Re}_{ef} - He^3 + 192He\,\mathrm{Re}_{ef}^{\,2} + 512\,\mathrm{Re}_{ef}^{\,3}\right)}{\sqrt{\zeta^6\left(He + 8\,\mathrm{Re}_{ef}\right)^6}}\right) \tag{6}$$

He is the Hedstrom number given by:

$$He = \frac{\rho\tau_o(D_h - D_p)^2}{\mu^2} \tag{7}$$

in which τ_o is the Bingham fluid yield stress. The term ζ in Eq. (5) is defined by:

$$\zeta = \frac{(1-\beta)^2}{(1+\beta^2) - \dfrac{(1-\beta^2)}{\ln\left(\dfrac{1}{\beta}\right)}} \tag{8}$$

where β represents a diameter ratio ($\beta = D_p / D_h$).

The effective Reynolds number, Re_{ef}, is evaluated according to:

$$\mathrm{Re}_{ef} = \frac{\rho V_{ef}(D_h - D_p)}{\mu} \tag{9}$$

being V_{ef} the effective computed as:

$$V_{ef} = \overline{V} + \kappa V_p \tag{10}$$

where $\overline{V}$ is the fluid average velocity and κ is a geometric parameter given by:

$$\kappa = -\left[\frac{1 - \beta^2 + 2\beta^2\ln\beta}{2(1-\beta^2)\ln\beta}\right] \tag{11}$$

2.1.2 Power Law Fluid

For the power law fluid, on the other hand, the shear stress computed by:

$$\frac{\pi}{A_t}\left(D_h\tau_h - D_p\tau_p\right) = -\chi\frac{k^2}{\rho(D_h - D_p)^3} \tag{12}$$

where k is the fluid coefficient of consistency. The parameter χ is a function of the Reynolds number and is given by:

$$\chi = C_{LP}\,\mathrm{Re}_{LP}^{\,n-1} + C_{LP}\,\mathrm{Re}_{LP}^{\,n-1}V_{vp}V_p \tag{13}$$

being n the power law index; C_{LP} is defined by:

$$C_{LP} = 16\frac{\zeta\,\mathrm{Re}_{LP}^{\,2-n}}{V_{ef}} \tag{14}$$

and Re_{LP} is the Reynolds number for power law fluids defined as:

$$\mathrm{Re}_{LP} = \frac{(D_h - D_p)^n V_{ef}^{\,2-n}\rho}{8^{n-1}k}\left(\frac{4n}{3n+1}\right)^n \tag{15}$$

2.1.3 Adimensionalisation

To reduce the number of variables, the governing equations are normalized according to the dimensionless parameters shown in Table 1. The dimensionless form of the state equation and the conservation equation of mass are thus written, respectively, as:

$$P^* = P^*_{atm} + \frac{1}{\alpha^*}\ln\rho^* \tag{16}$$

$$\frac{\partial(\rho^* V^*)}{\partial z^*} + \frac{\partial\rho^*}{\partial t^*} = 0 \tag{17}$$

The dimensionless form of the momentum conservation equation is written as:

$$\frac{\partial(\rho^* V^*)}{\partial t^*} + \frac{\partial(\rho^* V^* V^*)}{\partial z^*} = -\frac{\partial\rho^*}{\partial z^*} - \frac{1}{Fr}\rho^* - \frac{2\psi}{\rho^*}\frac{RA}{\mathrm{Re}^2} \tag{18}$$

where ψ can assume the value of ε_2 (Eq. (5)) or χ (Eq. (12)), depending on the type of fluid: Bingham or power law. The dimensionless groups in equations (16), (17) and (18) are defined in Table 2.

The initial conditions for velocity, density and pressure are given respectively by:

$$\overline{V}^*(z^*, t^* = 0) = 0 \tag{19}$$

$$\rho^*(z, t^* = 0) = \frac{1}{1 - \frac{\alpha^*}{Fr}(1 - z^*)} \tag{20}$$

$$P^*(z, t^* = 0) = P_{atm}{}^* + \frac{1}{\alpha^*}\ln\left[\frac{1}{1 - \frac{\alpha^*}{Fr}(1 - z^*)}\right] \tag{21}$$

The flow displaced by the drill pipe is taken as boundary condition at the bottom hole and therefore, fluid average velocity is defined as:

$$\overline{V}^*(z = 0, t) = \frac{\beta^2}{1 - \beta^2} \tag{22}$$

The density is constant and equal to its atmospheric condition value in the upper boundary by:

$$\left.\frac{\partial\left(\rho^*\overline{V}^*\right)}{\partial z^*}\right|_{z^*=1} = 0 \tag{23}$$

Table 1. Dimensionless parameters.

Dimensionless parameters	Definition
Position	$z^* = \frac{z}{L}$
Time	$t^* = t\frac{V_p}{L}$
Average Velocity	$\overline{V}^* = \frac{\overline{V}}{V_p}$
Density	$\rho^* = \frac{\rho}{\rho_{atm}}$
Pressure	$P^* = \frac{P}{\rho_{atm}V_p^2}$

Table 2. Dimensionless groups.

Dimensionless groups	Definition
Aspect Ratio	$RA = \frac{L}{(D_h - D_p)}$
Reynolds Number	$\mathrm{Re} = \frac{\rho_{atm}V_p(D_h - D_p)}{\mu}$
Froude Number	$Fr = \frac{V_p^2}{gL}$
Dimensionless Compressibility	$\alpha^* = \alpha\rho_{atm}V_p^2$

3. NUMERICAL MODEL

The governing equations are discretized by the Finite Volume Method (Maliska, 2004) and the discretization scheme is illustrated in Figure 3. Density and pressure are placed at the finite volume boundaries and the velocity is located at the center of the control volumes. The grid is uniform and Δz is constant. Changes of cross sectional area are always placed in the middle of a velocity control volume, which means that this finite volume has two different diameters. The resulting discretized momentum conservation equation is given as:

$$R_I \overline{V}^{*n+1}_I = S_I \overline{V}^{*n+1}_{I-1} + T_I \overline{V}^{*n}_I + U_I \tag{24}$$

where the coefficients R_I, S_I, T_I and U_I are described by different equations, depending on the geometrical position of the control volumes. For control volumes placed in the cross sectional variation, the coefficients are given by

$$R_I = \frac{\rho^{*n+1}_{i'+1} + \rho^{*n+1}_{i'}}{2}\frac{\Delta z^*}{\Delta t^*} + \left[1 + \left(1 - J\frac{A^*_1}{A^*_2}\right)^2\right]\rho^{*n+1}_{i+1}\left(\frac{\overline{V}^{*n+1}_{I+1} + \overline{V}^{*n+1}_I}{2}\right) \tag{25}$$

$$S_I = \rho^{*n+1}_{i'}\left(\frac{\overline{V}^{*n+1}_{I'} + \overline{V}^{*n+1}_{I'-1}}{2}\right) \tag{26}$$

$$T_I = \left(\frac{\rho^{*n}_{i'} + \rho^{*n}_{i'+1}}{2}\right)\frac{\Delta z^*}{\Delta t^*} \tag{27}$$

$$U_I = -\frac{1}{Fr}\left(\frac{\rho^{*n+1}_{i'} + \rho^{*n+1}_{i'+1}}{2}\right)\Delta z^* - \left(P^{*n+1}_{i'+1} - P^{*n+1}_{i'}\right) - \frac{4\varepsilon_2}{\rho^{*n+1}_{i'} + \rho^{*n+1}_{i'+1}}\left(\frac{RA_1}{\mathrm{Re}_1^2} + \frac{RA_2}{\mathrm{Re}_2^2}\right)\Delta z^* \tag{28}$$

where, $RA_i = \frac{L_i}{D_{h_i} - D_p}$, $\mathrm{Re}_i = \frac{\rho_{atm}V_p(D_{h_i} - D_p)}{\mu}$ and $\beta_i = \frac{D_{h_i}}{D_p}$ Subscript 1 and 2 refer to downwind and upwind cross sectional areas, respectively. In Eq. (25), J is a coefficient of local pressure drop which is equal to 1 for an expansion and equal to $J = -1.52\left(A_1/A_2\right)^3 + 2.19\left(A_1/A_2\right)^2 - 1.22\left(A_1/A_2\right) - 0.135 + 1.685\left(A_1/A_2\right)^{-1}$ (Assy, 2004) for a contraction.

4. RESULTS

This section starts with a grid size analysis, followed by the results validation and geometry analysis, where the effects of cross section changes are studied. Finally, after proceed a sensitivity analysis, a comparison between numerical and experimental results is presented.

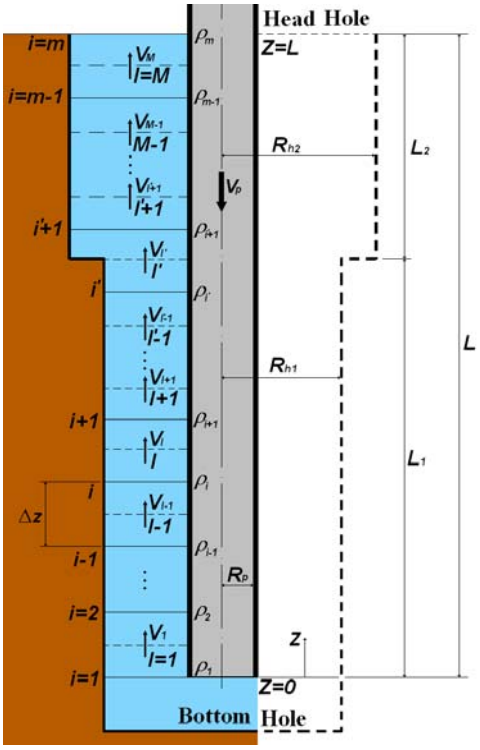

Figure 3. Discretization scheme of the numerical domain.

4.1 Grid Test

A sensitivity analysis of the grid size is first conducted for a reference case. In all simulations, a wellbore with only one cross sectional change is studied. The variation is placed in the middle of the well. Reference values of the dimensionless variables are $\alpha^* = 1.86\times10^{-7}$, $RA_1 = 33333$, $RA_2 = 20000$, $\mathrm{Re}_1 = 200$, $\mathrm{Re}_2 = 333$, $\beta_1 = 0.4$ and $\beta_2 = 0.2857$. For the Bingham fluid, the Hedstrom numbers utilized are: $He_1 = 4300$ e $He_2 = 11900$ and for a power law fluid, the index $n = 0.8$ is adopted.

According to Fortuna (2000), time and space grids have to satisfy the Courant-Fredrichs-Lewy (CFL) criterion because of the hyperbolic characteristic of the equations. The CFL number is kept equal to 0.25 for all case studies.

In the numerical experiments, grid cells with 10, 100, 200, 400, 600, 800 and 1000 volumes were tested. Results for the sensitivity analysis for Bingham and power law fluids are depicted in Figures 4 and 5, respectively. For convenience only results for 10, 800 and 1000 control volumes are presented. Note that "A" label symbolizes the pressure values at the bottom edge of the wellbore, where $z^* = 0.0$ and "B" label regards the region that contains a cross sectional variation ($z^* = 0.5$).

As can be noticed, the pressure fields become insensitive to the grid size for 800 finite volumes, as the results for 800 and 1000 finite volume are quite close. Therefore, an 800-volume-grid is used for the simulations hereafter for both fluids.

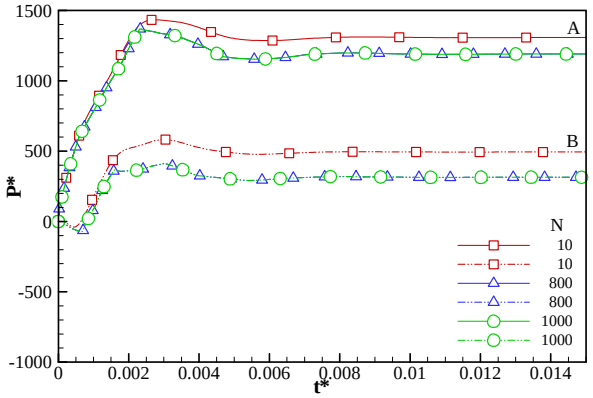

Figure 4. Historic pressure for three grid sizes (Bingham fluid).

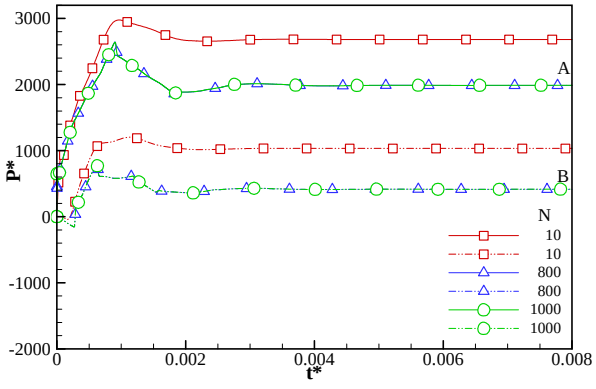

Figure 5. Historic pressure for three grid sizes (Power law fluid).

On the contrary to what is expected, the number of control volumes does not only affect the transient results but also the steady state values. As the cross sectional change is always placed at the center of a control volume, a grid refinement changes slightly the geometry.

4.2 Validation and geometric analysis

A comparison of the current model results with the results of a previous work (Almeida, 2009) is now conducted to verify the accuracy of numerical model. In this sense, a reference case with the following parameters was admitted: $V_p = 0.25\ [m/s]$, $L = 5575\ [m]$, $D_h = 0.2159\ [m]$, $D_p = 0.1143\ [m]$, $\rho = 1461.9\ [kg/m^3]$, $\mu = 0.35\ [Pa.s]$, $\alpha = 2.0\times10^{-9}\ [Pa^{-1}]$, $k = 0.35\ [Pa.s^n]$, $n = 0.8$, for power law fluid, and $\tau_o = 5\ [Pa]$, for Bingham fluid. Table 3 shows a good agreement of the results for a surge pressure at the bottom of the wellbore, providing credit to the current model.

The analysis of the effect of the cross-section change is now conducted. The results of a two-cross-section well are compared to those of a one-cross-section well. The later was obtained by Kimura (2008). In the cross-section change case, two situations were considered: an expansion and a contraction for the case of surge. For the expansion the diameter is two ($D_{h2} = 2D_{h1}$), whereas $D_{h2} = (2/3)D_{h1}$ for the contraction. For the sake of comparison, the drill pipe speed was adjusted to provide the same pressure at steady state. Figure 6 and 7 show the comparisons for Bingham fluid flow running in an expansion and a contraction, respectively. One can see that the results for the cross section variation present pressure peaks not observed for a uniform section well. Those peaks are due to pressure wave reflections that take place at the wellhead. In its way back to the bottom, the pressure wave passes through an annular region that is larger than that for the constant cross-sectional well. Thus, the pressure loss decreases and the pressure wave is reflected on a larger segment of the well, which in some cases can even reach the bottom of the well. Another effect is the pressure wave's reflection in the cross-section variation area, since in this region part of the wave is reflected and part is transmitted to the remainder of the wellbore. This phenomenon, added up with the reflection in the upper extremity leads to greater peaks in the transient period.

Considering that in the drilling process the annular cross-section at the wellhead is usually greater than downwards, the pressure prediction is rather important, as such cross-section change can lead the system behavior to critical situations in the transient regime. On the other hand, if such pressure goes toward a contraction, the pressure faces a minor annular region when returning. That explains the smoothed peaks observed in the contraction case. These results are quite similar to those of Power Law fluids.

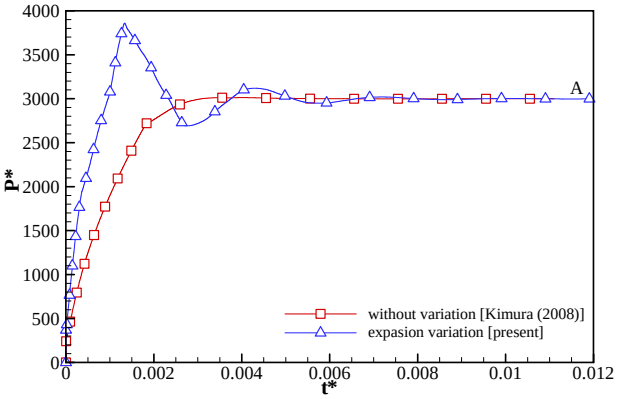

Figure 6. Comparison between an oil well with constant cross-sectional area and another with expansion.

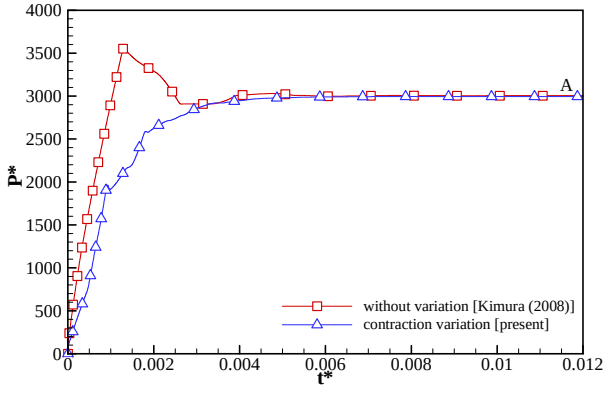

Figure 7. Comparison between an oil well with constant cross-sectional area and another with contraction.

4.3 Sensibility Analysis

In all following simulations, the case of one expansion in the middle of the well is focused. The effect of the Hedstrom number is analyzed and the results are shown in Figure 8 and 9. As shown in Figure 8, the increase of the Hedstrom number leads not only to an increase of both maximum and steady state pressures but also to a larger difference between the maximum and the steady state values. Figure 9 shows that raising the Hedstrom number also raises the pressure loss, although the difference between the pressure gradient before and after the cross-section variation remains.

The effect of the power law index was evaluated and the results are shown in Figures 10 and 11. Figure 10 shows that as the power law index approaches to zero, the fluid apparent viscosity decreases, so that the fluid demands less

energy to produce the same flow. As a consequence, the lower power law indexes the lower the pressure obtained. Such diminished power dissipation permits the pressure wave to propagate through a longer path. Indeed, that can be associated not only with the elevated number of peaks in the transient regime and but also with the longer time requested to reach the steady state regime. Figure 11 allows the conclusion that the increase of the index turns more evident the presence of the cross-section variation.

4.4 Comparison with experimental data

To demonstrate the applicability of the method here presented, a comparison between numerical and experimental data, obtained with the cooperation of Petrobras, was performed. These experimental tests were accomplished at the Taquipe – State of Bahia, where Petrobras holds an experimental rig, capable to monitor and control the drill pipe speed. In Table 4, information about the wellbore geometry and the rheology of the drilling fluid used during the tests is presented.

The rheology properties of the drilling fluid were obtained from a Fann 35A viscometer and fitted to the Bingham model. Since the fluid compressibility is not available, its value was adjusted to fit the measured and computed hydrostatic pressures. As the experimental well presents uniform annular region along its length, the numerical domain was set to follow this pattern.

Figure 12 compares the experimental and computed values of swab pressures. The measured drill pipe speed is $-0.225\,m/s$ and this value is fed into the model. In Figure 13, the comparison was conducted for a surge case in which the drill string speed was $0.618\,m/s$. Despite the good agreement of the swab case, the discrepancy observed in the surge case after 10s is quite considerable. The reason for that is the difficult to control and to maintain constant the drill pipe speed for the surge case. Notice that the numerical results seemed to be more conservative, as its critical values of pressure are higher than those obtained in the experimental tests.

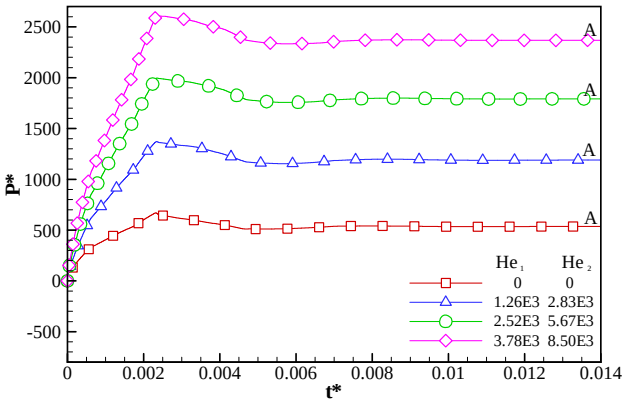

Figure 8. Historic pressure accounting four different Hedstrom numbers.

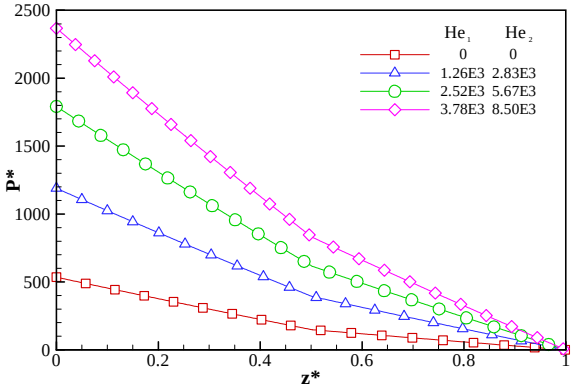

Figure 9. Pressure field accounting four different Hedstrom numbers.

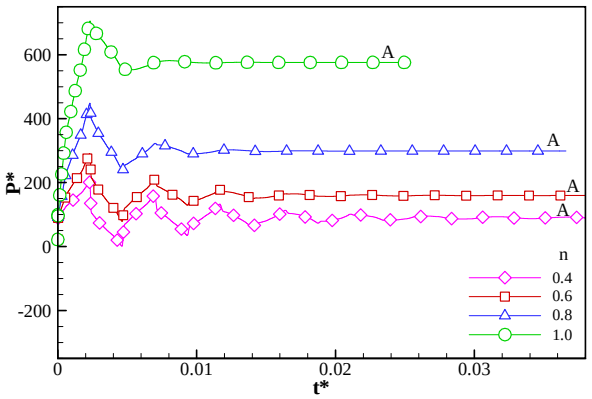

Figure 10. Historic of pressure field considering three Reynolds number at two different instants.

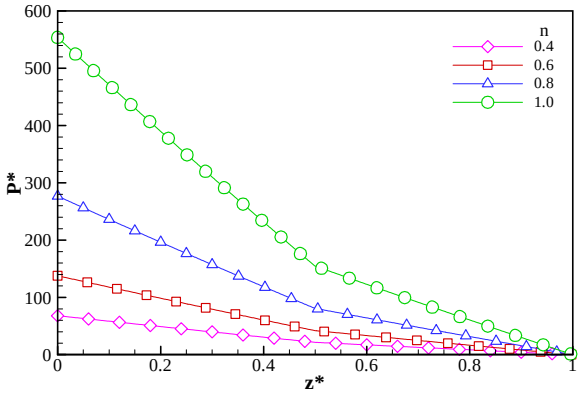

Figure 11. Pressure field considering three Reynolds number at a position near the head.

Table 3. Comparison between Almeida (2009) versus present work results.

	Surge Pressures [Pa]		
	Almeida (2009)	**Present**	**Error [%]**
Bingham	3,351,972.41	3,352,151.44	0.005
Power law	1,007,339.02	977,118.30	3.093

Table 4 – Geometry and rheological properties regarding the experimental tests conducted by Petrobras.

Parameter	**Value [Un.]**
Lenght (L)	1192 [m]
Wellbore diameter (D_h)	0.16848 [m] (6.633 pol)
Drill pipe diameter (D_p)	0.1143 [m] (4.5 pol)
Density (ρ_{atm})	1833.3 [kg/m^3] (15.3 lbm/gal)
Plastic viscosity (μ)	0.0738 [$Pa.s$]
Yield stress (τ_o)	9.0202 [Pa]

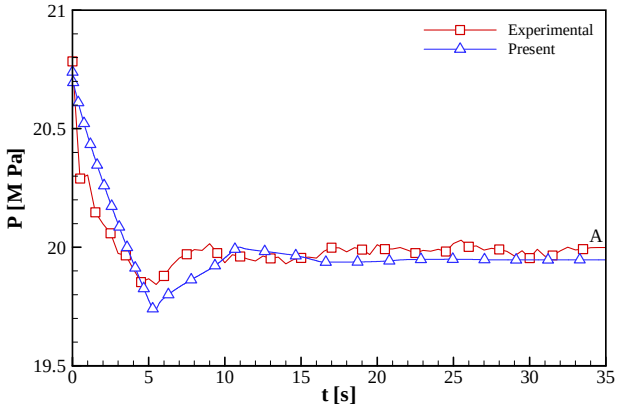

Figure 12. Historic of pressure: comparison between numerical and experimental results for a swab test.

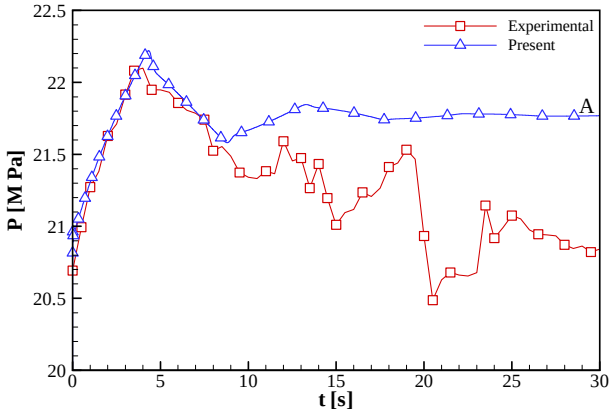

Figure 13. Historic of pressure: comparison between numerical and experimental results for a surge test.

5. CONCLUSION

In this paper, a mathematical model to predict surge and swab pressures in a vertical oil well with cross-section variation is presented. The fluid is modeled as non-Newtonian (Bingham and power law fluids) with constant compressibility. The flow is assumed to be isothermal, one-dimensional and laminar. All simulations were performed for two-cross-section wells. The governing equations are solved by the Finite Volume Method.

The cross-section variation alters significantly the pressure behavior in the transient regime in either surge or swab event. Not only the contraction but also the expansion in wells increases the pressure peaks in comparison to a constant cross-section well. Nevertheless, the effect of the expansion is larger than that of the contraction.

The increase of the Hedstrom number, for a Bingham fluid, also increases the pressure loss, although the difference between the pressure gradient before and after the cross-section variation is kept constant. For Power law fluids, the pressure loss decrease with the power law index.

The treatment of the equations in dimensionless form turned the numerical method stable and the use of relaxation parameters became unnecessary. Not only the computation time was reduced but the number of dependent parameters associated with the process.

The comparison of numerical results with experimental data suggests that the present numerical model can be a useful tool for prediction of the phenomenon.

6. ACKNOWLEDGEMENTS

The authors acknowledge the financial support of PETROBRAS and PRH-10/ANP.

7. REFERENCES

Almeida, F. T. G. M. C. Sub e Sobrepressões Geradas Pelo Movimento Axial Transitório de Colunas de Perfuração. Mechanical Engineering Departament, UTFPR, Brazil, 2009.

Anderson, J. D. Modern Compressible Flow: With Historical Perspective. 2. ed. Estados Unidos: McGraw-Hill, 1990.

Assy, T. M. Mecânica dos fluidos: fundamentos e aplicações. 2ª edição. Rio de Janeiro. Editora LTC, 2004.

Bing, Z.; Kaiji, Z.; Qiji, Y. Equations Help Calculate Surge and Swab Pressures in Inclined Wells. Oil & Gas Journal, v. 93, n. 38, 1995.

Bing, Z.; Kaiji; Z. Dynamic Model Predicts Well Bore Surge and Swab Pressures. Oil & Gas Journal, v. 94, n. 53, 1996.

Bird, R.B.; Armstrong, R.C.; Hassager, O. Dynamics of Polymeric Liquids - Fluid Dynamics. New York: Ed. John Wiley e Sons, v. 1, 1987.

Bourgoyne, A. T.; Millheim, K. K.; Chenever, M. E. Applied Drilling Engineering, Estados Unidos: Sociedade de Engenheiros de Petróleo (SPE), 1991.

Burkhardt, J. A. Wellbore Pressure Surges Produced by Pipe Movement. SPE Drilling Engineering, v. 13, 1961.

Fedevjcyk, J. V. Inclusão das Variações de Seção de um Poço/Coluna de Perfuração na Modelagem do Problema Transitório de Surge & Swab. Mechanical Engineering Departament, UTFPR, Brazil, 2010.

Fontenot, J. E.; Clack, R. K. An Improved Method for Calculating Swab and Surge Pressures and Circulating Pressures in a Drilling Well. SPE Drilling Engineering, v. 14, n. 5, 1974.

Fortuna, A. O. Técnicas Computacionais para Dinâmica dos Fluidos: Conceitos Básicos e Aplicações. 1. ed. São Paulo: São Paulo University, 2000.

Kimura, H. F. Modelagem Transitória do Escoamento de Fluido Newtoniano Gerado Pela Movimentação Axial de Colunas de Perfuração de Poços de Petróleo. Mechanical Engineering Departament, UTFPR, Brazil, 2008.

Lal, M. Surge and Swab Modeling for Dynamic Pressures and Safe Trip Velocities. In: IADC/SPE Drilling Conference, 1983.

Maliska, C. R. Transferência de Calor e Mecânica dos Fluidos Computacional. 2ª ed. Rio de Janeiro: LTC, 2004.

Mitchell, R. F. Dynamic Surge/Swab Predictions. SPE Drilling Engineering, v. 6, n.4, p. 325-333, set. 1988.

Oliveira, G. M. Reinício da Circulação de Fluidos de Perfuração em Espaços Anulares Horizontais. Mechanical Engineering Departament, UTFPR, Brazil, 2008.

Patankar, S. V. Numerical Heat Transfer and Fluid Flow. Hemisphere Publishing Corp, 1980.

Sampaio Jr., J. H. B. Aplicativo para Estimativa de Surge e Swab para Cenários UDW/formações frágeis. Report.

Thomas, J. E (Organizator). Fundamentos de Engenharia do Petróleo. 2. ed. Rio de Janeiro: Editora Interciência. 2004.

8. RESPONSIBILITY NOTICE

The authors are the only responsible for the printed material included in this paper.